Macromolecules

pubs.acs.org/Macromolecules Article

Effect of Graft Molecular Weight and Density on the Mechanical Properties of Polystyrene-Grafted Cellulose Nanocrystal Films

James H. Lettow, Han Yang, Paul F. Nealey,* and Stuart J. Rowan*

Cite This: *Macromolecules* 2021, 54, 10594−10604 Read Online

ACCESS | Metrics & More | Article Recommendations | Supporting Information

ABSTRACT: Polymer-grafted nanoparticle (PGN) films were prepared from polystyrene (PS) grafted to rodlike cellulose nanocrystals (***MxG*-CNC-*g*-PS**) with a controllable grafting density (0.03−0.25 chains/nm^2) and molecular weight (5−60 kg/mol). These nanorod-based PGNs are solution- and melt-processible, permitting access to one-component composite films with high nanofiller loadings (with up to 55 wt %). The impact of both grafted polymer density and molecular weight on the mechanical properties of the films was investigated and related to the polymer brush conformation: concentrated polymer brush (CPB), semidilute polymer brush (SDPB), or CPB core with SDPB corona (CPB/SDPB). The rubbery regime storage modulus (above T_g) showed 2 orders of magnitude increase, maximizing at a low degree of polymerization (N) and low grafting density (σ). Fracture toughness was maximized in samples with the grafted polymer in the SDPB or CPD/SDPB (higher N and relatively low σ) regime and showed enhancement relative to PS of molecular weight similar to the graft. In line with prior computation predictions, optimizing for both rubbery modulus and fracture toughness in such nanorod-based PGN films requires the polymers in the SDPB regime and CNC loading levels (ca. 50−60 wt %) that are difficult to attain in more traditional two-component CNC composites.

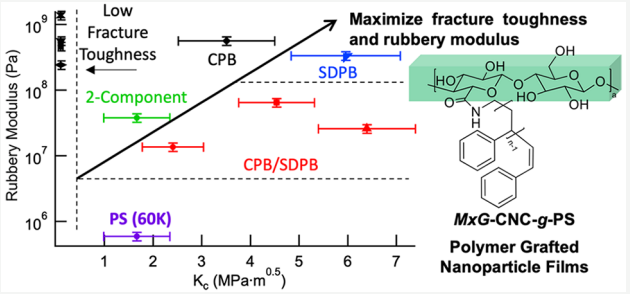

INTRODUCTION

Nanocomposites, in which a nanofiller is embedded in a polymer matrix, are used in a wide array of applications[1,2] in which an improvement in the polymer's material properties, for example, mechanical,[3−5] electronic,[6−8] water transport/purification,[9,10] and so forth, is required. The properties are often controlled by the ratio of polymer to nanofiller; however, such two-component nanocomposites often suffer from demixing/phase separation of the matrix and filler, which can lead to a reduction in the material properties, restrict possible processing techniques, and ultimately limit the loading of the nanofiller material. One way to address these issues is to covalently bond the polymer matrix to the nanoparticle filler, creating polymer-grafted nanoparticles (PGNs)[11] which can be processed into films solely consisting of PGNs, also known as one-component nanocomposites (OCNs).[12] Such OCNs can allow access to materials that exhibit enhanced toughness and modulus when compared to two-component nanocomposites of similar composition.[13,14] Furthermore, on account of the covalent bond between the polymer and nanofiller, these materials do not suffer from demixing, permitting melt processing and much higher loadings of nanoparticles beyond that of traditional nanocomposites.

The mechanical structure−property relationships of nanosphere-based OCNs have been studied in detail and are controlled by the graft polymer conformation.[13−16] In line with the traditional brush literature on planar surfaces,[17,18] radius of gyration (R_g) and polymer grafting density control the polymer brush conformation of OCNs based on spherical nanoparticles (Figure 1a), in which the polymer brush conformation falls into three regimes: mushroom, semidilute polymer brush (SDPB), and concentrated polymer brush (CPB) (Figure 1b).[12] The mushroom regime, where the grafted polymer exists in a loose coil conformation with little interactions between grafted chains, occurs when the polymer grafting density is less than R_g^{-2}. At slightly higher grafting densities (and/or higher molecular weights), the polymer brushes move into the SDPB regime in which the polymer chain conformations are still generally relaxed but now there are soft inter-graft interactions and chain penetration. PGNs in which the polymer is in the CPB regime, on the other hand, are more akin to hard particles. On account of curvature of the nanoparticle, an inner corona of CPB with an outer layer of SDPB, termed CPB/SDPB, is generally formed if the molecular weight of the polymer graft is large enough. Previous work[13−16] has confirmed densely packed brushes on spherical PGNs

Received: September 6, 2021
Revised: October 21, 2021
Published: November 14, 2021

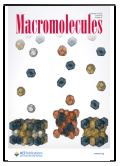

https://doi.org/10.1021/acs.macromol.1c01886
Macromolecules 2021, 54, 10594−10604

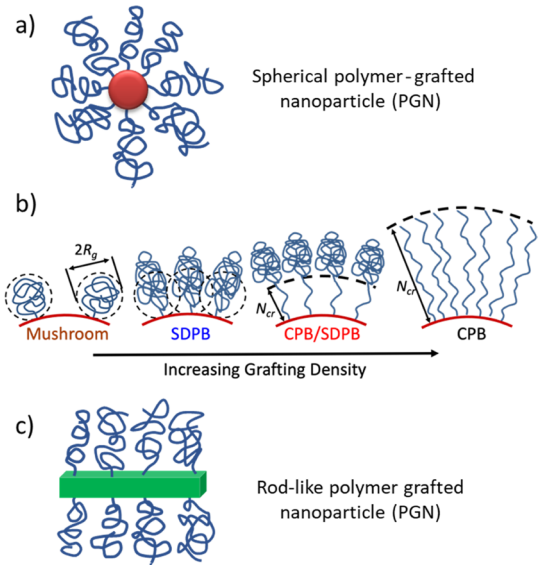

Figure 1. Schematic of (a) a spherical PGN, (b) a representation of the various polymer brush conformations on a curved surface upon increasing polymer grafting density (mushroom, SDPB, CPB/SDPB, and CPB), and (c) a rodlike PGN.

transition from CPB to CPB/SDPB at critical polymer lengths and grafting densities following predictions by Daoud−Cotton models applied to nanoparticles.[19−21] Additionally, the mechanical properties of spherical PGNs show increasing stiffness (elastic modulus) with the increase in molecular weight and increasing toughening behavior (via crazing) when polymer grafts reside in the CPB/SDPB regime with sufficient molecular weight to entangle.[13,15] Thus, the mechanical properties of OCNs are determined by the graft polymer conformation, which in turn is controlled by the polymer grafting density and radius of gyration. However, while much work has been done on nanosphere-based OCNs, much less work has investigated nanorod geometries (Figure 1c).

Cellulose nanocrystals (CNCs) are organic, biorenewable nanorods with a high degree of crystallinity and easily functionalizable surfaces and have been investigated as green nanofillers.[22−26] CNCs are commonly prepared by acid hydrolysis, such as hydrochloric acid (HCl), hydrobromic acid, sulfuric acid, and phosphoric acid, of natural cellulose at elevated temperatures.[27,28] The width of the CNCs is between 3 and 20 nm, and their length can be 100−1000 nm depending on both the bioresource, for example, wood, cotton, tunicate, or *Miscanthus x. Giganteus* (*MxG*), and isolation procedures.[29,30] In addition to being bioavailable, CNCs offer a number of advantages, that include low coefficient of thermal expansion, high elastic modulus, and biocompatibility,[23,27,31] making them attractive nanoparticles for composite materials. Indeed, while there are only a few reported studies on OCN films of polymer-grafted CNCs, there are a number of examples in the literature of polymer-grafted CNCs, whether for study in solution or for integration into nanocomposites for enhancing mechanical properties.[32−38]

Recently, Weder and co-workers reported CNC-based OCNs with high molecular polymer grafts (100−400 kg/mol) and moderate grafting density (0.04−0.15 chains/nm^2) and demonstrated toughness and elastic modulus enhancement consistent with previous spherical nanofiller-based OCNs.[39] OCNs containing up to 20 wt % CNC with grafted high glass transition temperature (T_g) poly(methyl methacrylate) display enhanced toughening while retaining a similar elastic modulus to the two-component nanocomposite of similar composition. Additionally, OCNs consisting of low T_g poly(hexyl methacrylate) show similar toughness but higher modulus as compared to a mixed two-component nanocomposite. More recently, PGN films consisting of CNCs grafted with poly(2-phenylethyl methacrylate) imbibed with ionic liquid were prepared and their mechanical properties and ion conductivity were measured.[40] These imbibed PGN films (30 wt % ionic liquid) exhibited an increase in both tensile strength and ionic conductivity relative to the mixed CNC, polymer, and ionic liquid nanocomposites. These materials probed relatively low molecular weights (6−20 kg/mol) and moderate to high grafting densities (0.10−0.43), and the grafted polymers were predicted to reside in the CPB or CPB/SDPB regimes. In neither of these studies was the effect of molecular weight nor grafting density explored. Interestingly, Lettow et al. showed that both degree of polymerization and grafting density affect the ion conductivity of hydrated PGN films of polyelectrolyte-grafted CNCs with a relatively high density of short polymer chains resulting in the highest conductivity, although no detailed mechanical studies were performed on these thin films.[41]

Recently, theoretical and computational work has been applied to CNC-based OCNs, permitting better polymer regime and mechanical property predictions. Specifically, computational work by Keten and co-workers using coarse-grained and molecular dynamics approaches, when combined with metamodels, have probed various design parameters (polymer chain length, grafting density, polymer−nanoparticle interaction strength, and the nanoparticle edge length) and their effects on the poly(methyl methacrylate) polymer brushes.[42] Based on the simulations, predictions were made on the polymer conformation transition point from CPB to CPB/SDPB as a function of polymer length and grafting density, which was extended in further work to a wide array of polymers including polystyrene (PS).[43] Additionally, modeling indicated that the modulus is maximized at a low grafting density and degree of polymerization (i.e., higher volume fractions of CNCs), while toughness is maximized at a relatively low grafting density but high degree of polymerization. The computational studies suggested that in order have both modulus and toughness maximized, the grafted polymer should be in the SDPB regime and the OCN should have a CNC content of ∼60 wt %. While the initial experimental work on CNC-based OCNs discussed above have shown that they can exhibit interesting properties, to date no work has been done to explore the effects that degree of polymerization and polymer chain density have on mechanical properties in support of these computational studies. To this end, reported herein are studies with the goal of synthesizing and studying PS-grafted CNC-based OCNs in order to probe experimentally the impacts that polymer grafting density and degree of polymerization have on the grafted polymer conformation and mechanical properties of their films.

EXPERIMENTAL SECTION

Materials. *Miscanthus x. Giganteus* were donated by Aloterra Energy LLC, Conneaut, Ohio, and ground before use. Styrene was purchased from Sigma-Aldrich and passed through a basic alumina column immediately before use. HCl and sodium hydroxide (NaOH)

https://doi.org/10.1021/acs.macromol.1c01886
Macromolecules 2021, 54, 10594−10604

were purchased from Fisher Scientific. All other reagents were purchased from Sigma-Aldrich and used as received.

Nuclear Magnetic Resonance Spectroscopy. The ^{1}H NMR and ^{13}C NMR spectra were recorded on a Bruker Ascend ADVANCE II+ 500 MHz spectrometer at 25 °C using $CDCl_3$ as solvent, and the NMR data were processed using MestReNova software.

Gel Permeation Chromatography−Multiangle Light Scattering and UV−Vis Spectrometry. Polymer molecular weight, dispersity, and UV−Vis spectra were recorded by gel permeation chromatography−multiangle light scattering (GPC−MALS) with in-line UV−Vis spectrometry using PL gel Mixed-D columns. The GPC−MALS was performed using a Shimadzu Prominence LC system equipped with a Wyatt Dawn Heleos MALS (658 nm laser) detector, a Wyatt Optilab T-rEX refractive index detector, and a Shimadzu SPD-M30A Photodiode Array detector (200−800 nm). High-performance liquid chromatography grade tetrahydrofuran (THF) was used as the eluent (1 mL/min) at 25 °C. The data were processed by Wyatt Astra software.

Conductometric Titration. The amount of surface carboxylic acid groups on the CNCs was determined by conductometric titrations using a Accumet XL benchtop pH/conductivity meter (Fisher Scientific). In a typical run, 25 mg of CNCs was dispersed in deionized (DI) water (80 mL) via sonication, and 15 μL of HCl (33 wt %) was added to adjust the pH to around 3. 0.01 M NaOH was then titrated into the CNC dispersion, and the conductivity was measured until the pH was around about 11.

Thermal Gravimetric Analysis. Thermal gravimetric analysis (TGA) experiments were carried out on a thermogravimetric analyzer (TA Instrument Discovery). The samples were heated from 30 to 650 °C under a nitrogen atmosphere with a heating rate of 10 °C/min.

Synthesis of α-Phthalimidomethyl-ω-butyltrithiocarbonatepoly(styrene) by RAFT. Phthalimidomethyl butyl trithiocarbonate (0.12 g) and styrene (16.6 g) were transferred to a 150 mL flask. The mixture underwent three freeze−pump−thaw cycles before being heated at 110 °C for 24 h. The mixture was then rapidly quenched to room temperature, diluted with THF (∼5 mL), and the resulting polymer was precipitated into methanol (100 mL), collected by filtration, and dried in a vacuum oven at 40 °C for 24 h. Two further precipitations from THF to methanol were used to remove the unreacted monomer yield and the desired α-phthalimidomethyl-ω-butyltrithiocarbonatepoly(styrene) (**PS-x**, where **x** denotes the molecular weight in kg/mol, as determined by GPC−MALS) after drying (in ca. 70% yield) ^{1}H NMR (500 MHz, $CDCl_3$); δ ppm: 7.8 (2H, Ar**H**, phthalimide), 7.7 (2H, Ar**H**, phthalimide), 7.2−6.3 (br PS) 3.4 (2H, N−CH_2−), 3.3 (2H, S−CH_2−), 2.2−1.2 (br PS), 1.0 (3H, −CH_3) (Figure S1). GPC−MALS (THF) PS-x series were measured (M_n = 5, 8, 12, 27, 34, 60 kg/mol, Đ < 1.1) (Figure S2). UV−Vis (THF) λ_{max} = 310 nm (trithiocarbonate end group) (Figure S3).

Synthesis of α-Aminomethyl-poly(styrene). α-Aminomethyl-poly(styrene) was synthesized following literature precedent.[44] α-Phthalimidomethyl-ω-butyltrithiocarbonatepoly(styrene) (1 g) was placed in a 150 mL beaker, and the polymer was heated at 250 °C under vacuum for 4 h. The polymer was dissolved in THF and precipitated into methanol three times, collected by filtration, and then dried in a vacuum oven at 40 °C for 24 h to yield 0.9 g (90% yield). ^{1}H NMR and UV−Vis confirmed the removal of the trithiocarbonate end group via reduction of peaks at 1.0 and 3.3 ppm and 310 nm, respectively (Figures S1 and S3). A peak in ^{1}H NMR at 6.0 ppm is indicative of the double bond formation at the PS end group. Additionally, TGA of low molecular weight PS confirmed end group removal by comparing weight loss (Figure S4). The resulting α-phthalimidomethyl-poly(styrene) was dissolved in THF (50 mL) and then hydrazine hydrate (5 mL) was added. The mixture was refluxed for 2 h, cooled to room temperature, and left overnight for precipitation. The liquid phase was then precipitated by pouring into methanol, collected by filtration, and dried in a vacuum oven at 40 °C for 24 h. Deprotection to form α-aminomethyl poly(styrene) (**PS−NH_2-x**, where **x** denotes the molecular weight in kg/mol as determined by GPC−MALS) was confirmed using a Kaiser test, GPC−MALS, and ^{1}H NMR. GPC−MALS (THF) confirms similar molecular weight after thermolysis, with all **PS-NH_2-x** samples shown in Figure S5 (5, 8, 12, 27, 34, and 60 kg/mol, Đ < 1.1). ^{1}H NMR (500 MHz, $CDCl_3$) δ ppm: 7.2−6.3 (br PS), 6.0 (1H, C═C−H), 3.4 (2H, N−CH_2−), 2.2−1.2 (br PS) (Figures S1 and S6). UV−Vis (THF) shows full reduction of the 310 nm peak (Figure S3)

Preparation of *MxG*-CNCs. ***MxG*-CNCs** were isolated from ground *Miscanthus x. Giganteus* stalks using HCl hydrolysis and were oxidized to yield ***MxG*-CNC-COOH** by TEMPO oxidation following published procedures.[30] Conductivity titration was performed to determine surface charge density, with ***MxG*-CNC-COOH** having surface charge density of ca. 1000 mmol/kg. TGA, wide-angle X-ray scattering (WAXS), and atomic force microscopy (AFM) confirm thermal decomposition, crystallinity index, and size, respectively (Figures S7−S9).

Preparation of a CNC/DMF Suspension by Solvent Exchange. ***MxG*-CNC-COOH** (2.5 wt %) was dispersed in 40 mL of water using ultrasonication. 1 mL of saturated NaCl was added, and the resulting gel was collected by centrifugation (5 min, 8000 rpm). The remaining gel was resoaked in 40 mL of methanol for 2 h with constant shaking before being separated by centrifugation. This procedure was repeated two more times with methanol and then two times with dimethylformamide (DMF). The concentration of the resulting ***MxG*-CNC-COOH**/DMF suspension (as determined by TGA) was ca. 0.25 wt %.

Electrospray Mass Spectroscopy. Electrospray mass spectroscopy (ESI−MS) experiments were conducted using an Agilent 6135 quadrupole LC/MS system equipped with a 50 × 4.6 mm Poroshell 120 EC-C18 column (Agilent). A gradient elution of 10−100% acetonitrile in H_2O (+0.1% TFA) was conducted over 10 min and then held at 100% acetonitrile for 2.5 min, and the absorbance was measured at 220 nm.

Preparation of $DMTMMBF_4$. To prepare **$DMTMMBF_4$**, *n*-methylmorpholine (2.4 mL) was added dropwise to a vigorously stirred solution of 2-chloro-4,6-dimethoxy-1,3,5-triazine (3.68 g in 40 mL H_2O) and kept stirring at 20 °C for 0.5 h. Then, a 30 mL sodium tetrafluoroborate (10 mmol) solution was added and stirred for another 2 h. The precipitate was collected by filtration and dried at room temperature to yield **$DMTMMBF_4$** in 75%. ^{1}H NMR (500 MHz, DMSO-d_6) δ ppm: 3.47 (s, 3H), 3.78 (m, 2H), 3.89, (m, 2H), 4.02 (m, 2H), 4.12 (s, 6H), 4.36 (m, 2H), ^{13}C NMR (125 MHz, DMSO-d_6); δ ppm: 53.1, 55.7, 57.2, 60.0, 61.8, 63.9, 170.6, 173.8, and ESI−MS (241, [M] + H−BF_4), agreeing well with the literature (Scheme S1, Figures S10 and S11).[45]

Example Synthesis of *MxG*-CNC-*g*-PS-5-45. $DMTMMBF_4$ (0.28 g) was added to a 40 mL suspension of ***MxG*-CNC-COOH** in DMF (0.25 wt %, 100 mg), obtained using the solvent exchange process, and the suspension was stirred at room temperature for 10 min. **PS-NH_2-5** (0.5 g for 5 kg/mol polymer) was dissolved in 10 mL of DMF and then added to the CNC suspension, and the reaction mixture was continuously stirred at room temperature for 24 h. The mole ratio of **$DMTMMBF_4$**: **PS-NH_2-5**: −COOH on CNCs was kept at 1:1:1. The resulting mixture was precipitated into methanol to yield a white precipitate. To remove any unreacted polymer, the precipitate was collected by centrifugation and redispersed in acetone by sonication, followed by further centrifugation to separate the precipitant and the supernatant. This was repeated three times or until a negative Kaiser test on the supernatant was obtained. ***MxG*-CNC-*g*-PS** was characterized with TGA and were shown to yield ***MxG*-CNC-*g*-PS-5-45**, where 5 refers to the molecular weight (5 kg/mol) and 45 refers to the weight percent of grafted PS.

The same procedure using reduced equivalents of polymer enabled access to PGNs with a lower amount percent of grafted polymer. Specifically, 0.25 equiv of **PS-NH_2-34** yielded ***MxG*-CNC-*g*-PS-34-80** and **PS-NH_2-60** yielded ***MxG*-CNC-*g*-PS-60-90**, while 0.04 equiv of **PS-NH_2-34** was used to access ***MxG*-CNC-*g*-PS-34-55**.

Film Formation. The ***MxG*-CNC-*g*-PS** samples were dissolved in THF and sonicated in a Branson CPX sonication bath before being cast into Teflon dishes. The solvent was allowed to evaporate at RT

https://doi.org/10.1021/acs.macromol.1c01886
Macromolecules 2021, 54, 10594−10604

for 2 days, followed by 1 day at 140 °C in a vacuum oven. After casting, films were melt-pressed at 140 °C for 30 min under 70 MPa.

Wide-Angle X-ray Scattering. The degree of crystallinity was determined by Synchrotron WAXS experiments performed at the DND-CAT 5-ID-D beamline of the Advanced Photon S3 Source (Argonne National Laboratory, Argonne, IL) using a triple detector system for simultaneous data collection SAXS and WAXS regimes. Two-dimensional data were collected on Rayonix CCD area detectors using an exposure time of ca. 0.1 s. Gaussian deconvolution and crystallinity index analysis followed literature precedent.[31]

Fourier Transform Infrared Spectroscopy. Fourier transform infrared spectroscopy (FTIR) spectra were recorded on a Shimadzu FTIR instrument. Solid samples were placed directly on the ATR crystal, and then, the spectra were recorded from 550 to 4000 cm^{-1} (and averaged over 46 scans) with a resolution of 4 cm^{-1}.

Atomic Force Microscopy. The dimensions of ***MxG*-CNC-COOH** and ***MxG*-CNC-*g*-PS** were investigated by Asylum Research Oxford Instruments Cypher ES AFM. A drop of the CNC suspension (0.01 wt %) was placed on a freshly cleaved mica surface which was pretreated with poly-*l*-lysine solution and then rinsed off after 5 min. The images were acquired using the AC Tapping mode. The sizes of nanoparticles were analyzed by Gwyddion software.

Scanning Electron Microscopy. Scanning electron microscopy (SEM) images of the cast films were taken with the Carl Zeiss−Merlin field emission scanning electron microscope. The acceleration voltage was 1.0 kV with a working distance of 2−3 mm using an in-lens detector. Two nanometers of Pt/Pd was sputtered onto the surface of the device using the Cressington 108 Auto Sputter Coater to reduce electron beam charging and improve the image quality.

Differential Scanning Calorimetry Analysis. Differential scanning calorimetry (DSC) experiments were performed on a TA Instruments Discovery DSC 2500. Samples (5−10 mg) were hermetically crimped in Tzero aluminum pans. Sequential heating, cooling, and reheating ramps were conducted from −50 to 200 °C at a rate of 10 °C min^{-1}.

Dynamic Mechanical Analysis. Dynamic mechanical analysis (DMA) experiments were conducted in the tension mode at a fixed frequency of 1 Hz using an RSA-G2 solid analyzer (TA Instruments). The CNC films were cut into a rectangular shape with about 4 mm in width and 10 mm in length. The temperature scan was performed between 20 and 200 °C with a heating rate of 3 °C/min.

Nanoindentation. Nanoindentation experiments were performed on a Hysitron Triboindenter using a Berkovich indenter. Samples were indented using displacement control to 1000 nm at a rate of 200 nm/s. AFM images of indentations were acquired using the same instrument.

Shear Rheology. Rheology was performed using the TA Instruments RSA-G2 ARES with a Forced Convection oven (20−200 °C) running TA Trios Software with a heating rate of 3 °C/min. An 8 mm parallel plate was used for all tests.

RESULTS AND DISCUSSION

In order to synthesize poly(styrene)-grafted CNCs, amide chemistry was utilized to graft amine-capped poly(styrene) (**PS−NH_2**) to carboxylic acid CNCs (***MxG*-CNC-COOH**). RAFT polymerization of styrene with phthalimidomethyl butyl trithiocarbonate[44] as the chain transfer agent (CTA) was used to produce the CTA-end-capped PS, which after thermal removal of the trithiocarbonate end group and subsequent deprotection of the amine yielded the targeted **PS-NH_2** (Scheme 1). A series of different molecular weight **PS-NH_2** (5, 8, 12, 27, 34, and 60 kg/mol, dispersity, Đ < 1.1, termed **PS-NH_2-x**, where x is the molecular weight in kg/mol) was prepared to range from 0.5 to 6 times the PS entanglement molecular weight (∼10 kg/mol) by simply varying the monomer-to-CTA ratio. The polymers were characterized by gel permeation chromatography multiangle light scattering (GPC−MALS), nuclear magnetic resonance spectroscopy (^{1}H NMR), and UV−Vis spectroscopy. ^{1}H NMR confirmed end group removal (both trithiocarbonate and phthalimide) (Figures S1 and S6). GPC−MALS measured the molecular weights and confirmed similar values before and after thermolytic cleavage of the trithiocarbonate moiety (Figures S2 and S5 and Table S1). UV-Vis showed reduction in the 310 nm peak corresponding to the trithiocarbonate moiety (Figure 3). TGA confirmed the thermal removal of the trithiocarbonate moiety when held at 250 °C for 4 h (Figure S5).

Scheme 1. Synthesis of PS-Grafted CNCs (*MxG*-CNC-*g*-PS-*x*-*y*), Where *x* Is the Molecular Weight (in kg/mol) and *y* Is the Percent Weight Fraction of the Grafted Polymer[a]

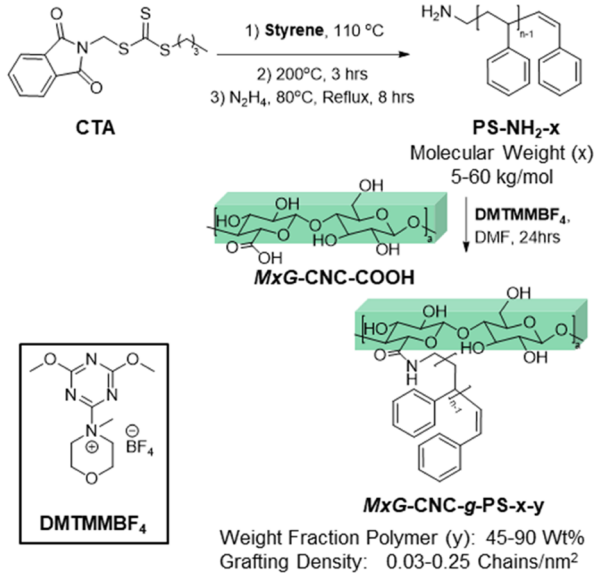

[a]The amine-end-capped poly(styrene) (**PS−NH_2-*x***) was prepared via RAFT polymerization and grafted to carboxylic acid-functionalized CNCs (***MxG*-CNC-COOH**) via peptide coupling chemistry before being cast into films via evaporation and pressed at 140 °C for 30 min under 70 MPa.

Coupling of the **PS-NH_2** to the CNCs via amide chemistry requires the use of the carboxylic acid-functionalized CNCs, which were obtained from *Miscanthus x. Giganteus* (via HCl hydrolysis and TEMPO-mediated oxidation) using literature procedures.[30] The resulting ***MxG*-CNC-COOHs** have a crystallinity index of 85% (determined by WAXS, Figure S8) and a carboxylic acid density of ca. 1000 mmol/kg, as determined via conductometric titration. The dimensions of the ***MxG*-CNC-COOHs** agree with the literature (from AFM, height = 2.2 ± 0.5 nm, length = 290 ± 60 nm for ***MxG*-CNC-COOH**, respectively (n = 20), Figure S9). The ***MxG*-CNC-COOHs** were dispersed in water using ultrasonication, followed by solvent exchange into methanol from the aqueous dispersion and subsequent solvent exchange into DMF. DMF was chosen as the solvent for the coupling reaction as it readily dissolves the polymer and disperses the CNCs. Various amide coupling reagents (DIC/NHS, DIC/HOBT, EDC/NHS) and reaction conditions (with direct mixing of CNCs in DMF or with CNCs in DMF prepared by solvent exchange) were explored (Schemes S1 and S2), and 4-(4,6-dimethoxy-1,3,5-triazin-2-yl)-4-methylmorpholinium tetrafluoroborate (**$DMTMMBF_4$**)[45] with CNCs dispersed using a solvent exchange process (Figures S10 and S11) was found to yield the highest grafting efficiency (Figure S12 and Table S2).

https://doi.org/10.1021/acs.macromol.1c01886
Macromolecules 2021, 54, 10594−10604

Thus, **DMTMMBF$_4$** was used to attach the different molecular weight (5−60 kg/mol) amine-end-capped **PS-NH$_2$-*x*** (x = 5, 8, 12, 27, 34, 60) onto the surface carboxylic acid groups of ***MxG*-CNC-COOH**. After purifying the samples to remove the ungrafted polymer via three cycles of centrifugation, decanting, and redispersion using acetone, the final samples were subjected to a Kaiser test to confirm that most of the free (ungrafted) polymer had been removed following previously published literature procedures.[40] An identical purification method was also shown efficacious in removing free, ungrafted polymer.[41] The sensitivity of the Kaiser test allows confirmation that the 60 kg/mol grafted samples contain less than 6 wt % free polymer, while the 12 and 5 kg/mol grafted samples have less than 1.2 and 0.5 wt % of ungrafted, free polymer, respectively. FTIR was used to confirm the presence of the new −CONH− bond (at 1650 cm^{-1}) in these PGNs (Figure S13).

AFM height images (Figure 2a,b) and the height profile (Figure 2c) of the ***MxG*-CNC-COOHs** and the ***MxG*-CNC-*g*-PS-8-*y*** PGN (grafted with **PS-NH$_2$-8**) show a height increase from 2.2 ± 0.5 to 4.5 ± 0.4 nm upon attachment of the polymer to the CNCs. See Figures S14 and 15 for AFM images

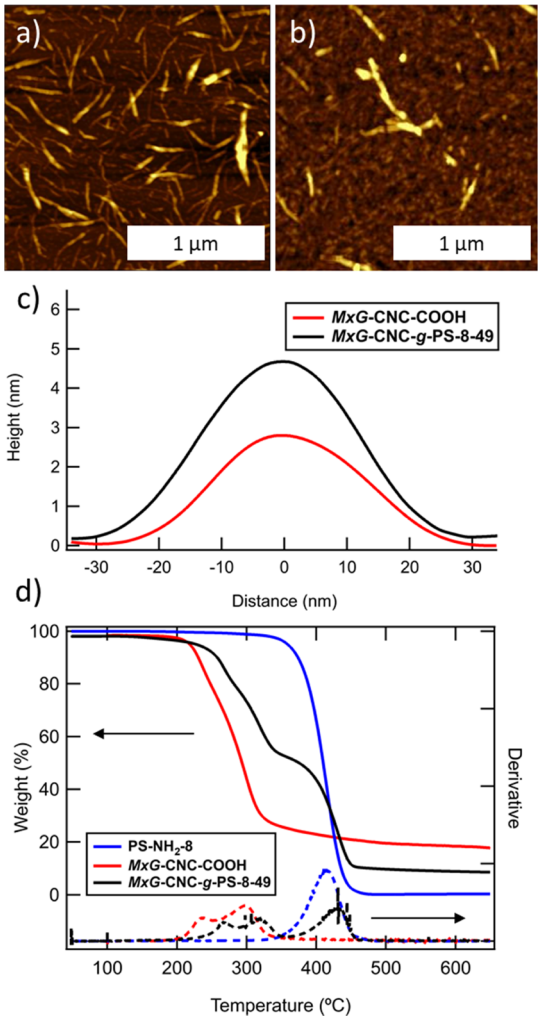

Figure 2. AFM height images of (a) ***MxG*-CNC-COOH** and (b) ***MxG*-CNC-*g*-PS-8-49** and (c) the AFM height profiles obtained from these images. (d) TGA of **PS-NH$_2$-8**, ***MxG*-CNC-COOH**, and ***MxG*-CNC-*g*-PS-8-49**.

of all the ***MxG*-CNC-*g*-PS** materials prepared. TGA was used to calculate the weight percent of the grafted polymer in the PGN. In the TGA, the PGNs (Figure 1d for ***MxG*-CNC-*g*-PS-8-*y***) show two clear regimes that correspond to the degradation of the CNC and PS. Comparing the mass loss from 220 to 360 °C (predominantly CNC degradation) to that of 360−450 °C (predominantly PS degradation) the weight percent of the grafted polymer can be estimated. After determining the weight percent of the polymer, ***MxG*-CNC-*g*-PS-8-*y*** is now termed ***MxG*-CNC-*g*-PS-8-49**, where the 8 is the molecular weight of the grafted polymer in kg/mol and the 49 is the weight percentage of polymer. Table 1 shows the data

Table 1. Sample Information of PS-Grafted Cellulose Nanocrystals with Associated Symbols Used in Subsequent Figures

***MxG*-CNC-*g*-PS-x-y**	Molecular Weight (kg/mol)[a]	Weight % Polymer[b]	Graft Density (Chains/nm^2)[c]
x - 5, y - 45 ⧓	5	45	0.15
x - 8, y - 49 ⧒	8	49	0.11
x - 8, y - 57 ▼	8	57	0.15
x - 12, y - 61 ◆	12	61	0.11
x - 12, y - 69 ◂	12	69	0.17
x - 27, y - 88 ●	27	88	0.25
x - 34, y - 55 ◤	34	55	0.03
x - 34, y - 80 ■	34	80	0.11
x - 60, y - 90 ▲	60	90	0.13

[a]From GPC−MALS. [b]From TGA. [c]See Supporting Information and ref 41 for details of the calculation.

on all the ***MxG*-CNC-*g*-PS** materials prepared along with their calculated grafting density (obtained from the polymer molecular weight and wt.%) following the literature procedure (see the Supporting Information for more details on page S13).[41]

Using the molecular weight determined by GPC−MALS and the calculated grafting density of the polymer on the CNC, the graft polymer conformation can be determined by comparing with the simulation data of poly(styrene)-grafted CNCs by Keten and co-workers.[42,43] As a note, the cross sections of CNCs are dependent on cellulose source and processing but generally are more parallelogram-like.[27,30] However, as the polymer radius of gyration is similar to or greater than the ***MxG*-CNC** dimensions, the surface will be considered to be effectively curved for the following calculations. For curved surfaces the polymer conformation can be predicted to be in either a mushroom regime, with no interaction between surface polymer grafts, or in a polymer brush regime. This transition can be estimated to occur at

$$\sigma = (\pi R_g^{\,2})^{-1} \quad (1)$$

where σ is the grafting density of the material in chains/nm^2 and the radius of gyration of the grafted polymer is $R_g \approx N^{0.5}$, with N being the degree of polymerization. When the grafting density is above this critical value, the polymer brush can be further subdivided into SDPB and CPB. For brushes on particles (as opposed to flat surfaces), the curved nature of the particles can result in polymer grafts which have an inner core of CPB and an outer corona of SDPB, termed CPB/SDPB. From Keten and coworkers,[42,43] the critical degree of polymerization (N_{cr}) as a function of grafting density for the

https://doi.org/10.1021/acs.macromol.1c01886
Macromolecules 2021, 54, 10594−10604

polymer to transition between CPB and CPB/SDPB can be estimated by the following equation

$$N_{cr} = \frac{2r_0}{3a\sigma_0^{*1/2}l_m}(r_0^{-3/4}\sigma_0^{*3/4}b^{3/2} - 1) \quad (2)$$

where r_0 is the radius of the CNC, a and b are fitting parameters from the computational modeling, l_m is the contour monomer length, and σ_0^* is a dimensionless grafting density given by

$$\sigma_0^* = \frac{fl_m}{2\pi r_0} = \sigma L l_m \quad (3)$$

where f is the number of polymer grafts, σ is the grafting density calculated in chains/nm^2, and L is the average length of the nanorod, 300 nm.[30] ***MxG*-CNCs** are known to have a ribbon-like cross section with height ca. 2.8 nm and width 8.5 nm, so a radius of 2.75 nm was used for r_0 to approximate the cross-sectional area (Figure S16). The fitting parameters (a = 2 and b = 35.34 A$^{0.5}$) and contour length (l_m = 2.57) are from Hansoge and Keten.[43] The intersection of the mushroom transition line (eq 1) and the CPB to SDPB transition line (eq 2) provides a critical grafting density below which the brush conformation is either mushroom at low molecular weight (or degree of polymerization) or SDPB at high molecular weights. Using this, the data from Table 1 can be converted into a phase diagram (Figure 3a) which defines the various grafted polymer conformation regimes.

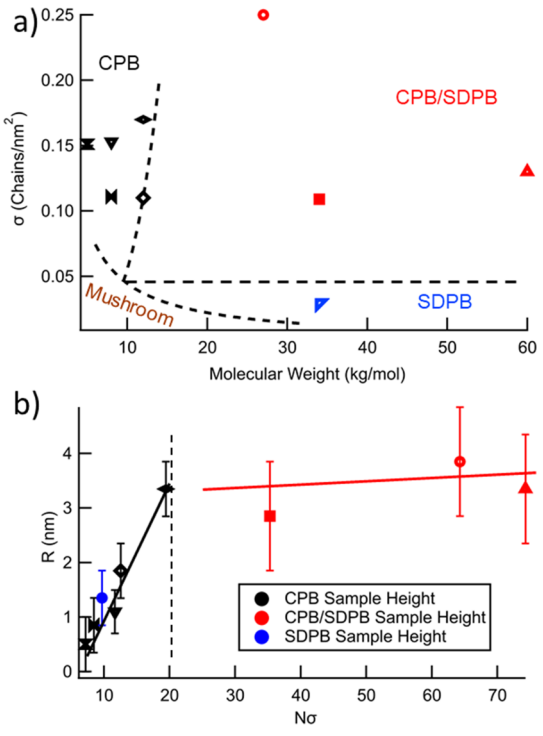

Figure 3. (a) Phase space mapping the ***MxG*-CNC-*g*-PS** sample molecular weight, grafting density, and polymer brush conformation consisting of CPB, CPB with SDPB corona (CPB/SDPB), and SDPB and (b) brush height, R, of ***MxG*-CNC-*g*-PS** samples plotted against the product of degree of polymerization and grafting density, with error from standard deviation of N = 10 and lines provided to guide the eye. See Table 1 for symbol designation.

The grafted polymer confirmations shown in the phase diagram in Figure 3a are based on the simulations and not experiments. However, Keten and co-workers[42,43] do provide relationships between degree of polymerization, grafting density, and predicted brush height that changes with conformation regime and can be experimentally examined. Specifically, they define the brush height, R, as

$$R = \frac{0.1abLl_m^2\sigma}{r_0^{0.5}}\left(\frac{N}{N_{cr}}\right)^x \quad (4)$$

where N is the degree of polymerization for the given polymer graft, x = 1 in the CPB regime or 0.5 in the CPB/SDPB regime, and N_{cr} being defined by eq 2. The measured height of the PGNs on mica (H_{PGN}) by AFM (Figures S14 and S15) consists of two layers of grafted polymer (top and bottom) plus the CNC height (H_{CNC}), allowing the experimental determination of the brush height, R [= (H_{PGN}−H_{CNC})/2]. Plotting this experimentally determined brush height versus $N\sigma$, it is possible to determine the transition between brush conformations. Plotting R as shown in Figure 3b, a straight line can be drawn through the samples with a $N\sigma$ of less than 20. If these PGNs are in the CPB regime, then x = 1, and the slope will equal $0.1abLl_m^2/r_0^{0.5}N_{cr}$, where N_{cr} is fixed at 120, the average value of N_{cr} for the ***MxG*-CNC-*g*-PS** samples in the CPB regime (calculated from eq 2). The slope of the line obtained from the experimental data is 0.172 ± 0.035 (Figure S17), which compares to 0.256 ± 0.091 based on the simulation work.[43] It is worthwhile noting that the simulation data involve polymer−polymer and polymer−CNC interactions, while the measured height from AFM involves polymer−air interactions, which presumably results in a more condensed PS brush (something that has been shown in literature for the AFM of other PGNs).[46] Figure 3b also clearly shows that above $N\sigma$ of 20, there is a significant change in the slope consistent with a change in the polymer conformation (from CPB to SDPB/CPB) above this value.

SEM image of the as cast and melt-pressed (at 140 °C for 30 min under 70 MPa) films offers some insights into the morphology of these ***MxG*-CNC-*g*-PS** materials. Specifically, Figure 4 shows individualized nanoparticles in as-cast samples up to graft molecular weights of ca. 34 kg/mol. Melt-pressing of these samples results in more continuous films unless the molecular weight of the graft is low, ca 5 kg/mol. After melt-pressing, both ***MxG*-CNC-*g*-PS-5-45** and ***MxG*-CNC-*g*-PS-60-90** show similarly low levels of porosity (Table S3). The difference in morphology can been seen in the optical images of the films, with the films consisting of individualized nanoparticles being opaque and the continuous films being more optically transparent. Interestingly, all the PGNs, even those that have very high weight percentage (55 wt %) of CNCs, form mechanically robust, processable materials.

Having confirmed the grafted polymer conformation and accessed robust PGN films, the mechanical properties of PGN materials were then investigated. To this end, it was decided to explore the modulus and toughness of the melt-pressed ***MxG*-CNC-*g*-PS** films which gave more reproducible results compared to the as-cast samples. Keten and co-workers predicted that low grafting density (σ) and low degree of polymerization (N) maximize modulus, while low grafting density and high degree of polymerization maximize toughness.[42] Figure 5a shows the storage modulus versus temperature from tensile DMA of the various ***MxG*-CNC-*g*-PS** films

https://doi.org/10.1021/acs.macromol.1c01886
Macromolecules 2021, 54, 10594−10604

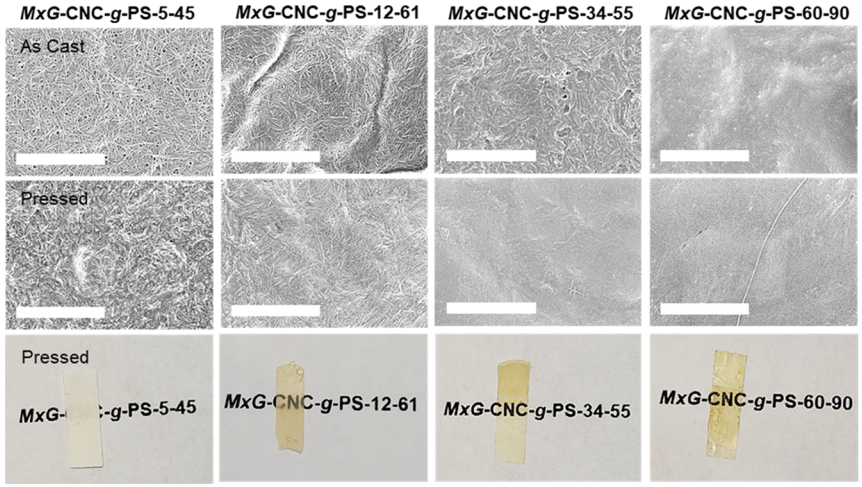

Figure 4. SEM images (scale bar 2 μm) and optical images of ***MxG*-CNC-*g*-PS-5-45**,***MxG*-CNC-*g*-PS-12-61**,***MxG*-CNC-*g*-PS-34-55**, and ***MxG*-CNC-*g*-PS-60-90** showing both as-cast and after melt-pressing at 140 °C for 30 min under 70 MPa.

with similar grafting densities (0.11 chains/nm^2) but different graft degrees of polymerization. As expected, the data show that with the increase in molecular weight (8−60 kg mol^{-1}) and therefore lower weight fraction of the CNC (51−10%) in the PGNs, there is a reduction in the modulus above glass transition temperature (T_g). For context, the melt-pressed **PS-NH$_2$-60** film and a mixed, two-component nanocomposite consisting of **MxG-CNC-COOH** with 90 wt % **PS-NH$_2$-12** are shown as controls. Relative to **PS-NH$_2$-60** the PGNs show a significant enhancement in modulus above T_g, while the mixed, two-component nanocomposite shows a similar modulus to that of the ***MxG*-CNC-*g*-PS-60-90** film. The main advantage of the PGN architecture when it comes to modulus is the ability to access homogeneous films with significantly higher nanofiller loading and therefore reinforcement. It is worthwhile noting that it was not possible to access homogeneous two-component films using solution-based (DMF) processing conditions with higher CNC loadings (beyond 10 wt %) similar to that accessed by the PGN films, consistent with the literature.[47]

Figure 5b shows the rubbery and glassy moduli (at $T_g \pm 20$ °C) plotted (from the tensile DMA data) versus $N\sigma$ for all the films. The data show that in the glassy state ($T < T_g$), the samples have only a slight dependence on $N\sigma$ with average modulus values of 2.0 GPa, while above T_g higher moduli tracks with a higher weight percent loading of CNC (or lower $N\sigma$) from 13 MPa to 1.37 GPa (Figure S18). This behavior is consistent with what is observed in other CNC-based nanocomposites,[47,48] where little reinforcement is seen in the glassy regime as the reinforcing CNC is of similar modulus to the glassy polymer while showing significant reinforcement in the rubbery regime with the increase in nanofiller content.[47,49]

The glass transition temperature (T_g) of the PGN system does show a remarkable increase compared to the PS homopolymer, particularly with the lower molecular weight grafts. Figure 5c shows the T_g of the ***MxG*-CNC-*g*-PS** films and corresponding **PS-NH$_2$** as a function of the PS (homopolymer or graft) molecular weight. While T_g was obtained from the peak of tan(delta) for all the materials, tensile DMA was used for the PGNs and oscillatory shear rheological measurements were used for the homopolymers (Figures S19 and S20). The T_g of the **PS-NH$_2$-60** film obtained by both shear rheology and tensile DMA was the same (Figure S21). The lowest molecular weight-grafted PGN films (5 kg/mol) have a T_g value 20 °C above the corresponding homopolymer. This difference decreases as the molecular weight increases such that at higher molecular weights, the PGN films have a $T_g \sim 1$ °C above the corresponding polymer. The impact of grafted polymer and nanocomposite interfaces on the T_g has been widely studied and largely shows higher T_g in nanocomposites and PGN-grafted systems, on account of (1) loss of chain end mobility and free volume, (2) confinement of the polymer system, and (3) polymer−substrate interactions.[50−55] Even so, while a 20 °C increase in T_g is not without precedent in model confined polymer interface systems,[51] it is among the higher in literature reported values observed in PGNs. It is also worthwhile noting that in the polymer-grafted CNCs that have similar molecular weight grafts at different densities, there does appear to be a slight increase (1−3 °C) in T_g in the higher grafting density materials, as can be seen in Figure 5c with the 8 and 12 kg/mol grafted samples.

Nanoindentation of the ***MxG*-CNC-*g*-PS** films was used to analyze the material properties and fracture toughness of the films. Figure 6a shows characteristic load−displacement curves of PGN films with a similar grafting density. By analyzing and fitting the unloading curves, the modulus (E) and hardness (H) can be obtained (Figure S22). The modulus follows similar trends as the glassy modulus of the PGN films shown in Figure 5b, while the hardness varies between 0.1 and 0.4 MPa. Upon indentation, the residual impression (and any cracks formed) can be used to determine the fracture toughness. ***MxG*-CNC-*g*-PS** films with 5, 8 kg/mol, and higher grafting density 12 kg/mol (***MxG*-CNC-*g*-PS-12-69**) polymer did not leave a distinct trigonal indentation and instead displayed major crack formation in the material, characteristic of a low fracture toughness material. All these easily fractured films comprise PGNs with CPB grafts. By contrast, a majority of the SDPB or CPB/SDPB ***MxG*-CNC-*g*-PS** films show a trigonal indentation (expected due to the Berkovich tip) with cracks extending from the corners of the indentation that are on the order of or less than the size of the Berkovich tip center to corner length (Figure S23). Analyzing the indentation and crack formation via AFM (Figures 6b and S23), the fracture toughness, K_c, can be quantified by

https://doi.org/10.1021/acs.macromol.1c01886
Macromolecules 2021, 54, 10594−10604

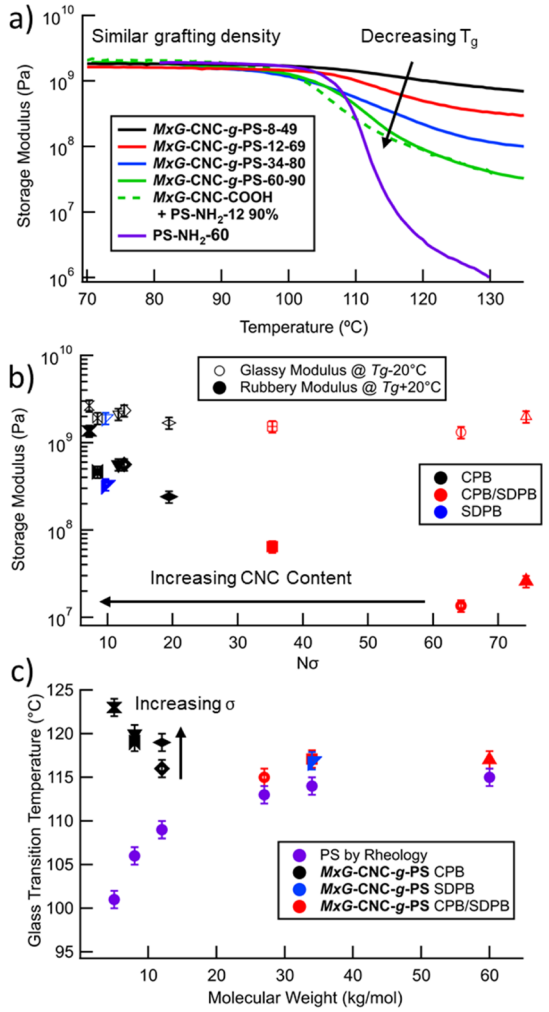

Figure 5. (a) Tensile DMA of select ***MxG*-CNC-*g*-PS** samples of similar grafting density (0.11 chains/nm^2), (b) storage moduli in the glassy regime (20 °C below T_g) and in the rubbery plateau (20 °C above T_g) plotted vs product of degree of polymerization and grafting density, with error from standard deviation of N = 3, and (c) T_g plotted vs molecular weight of both the PGN system and PS homopolymer, as determined by shear rheology for the homopolymer and from tensile DMA for the PGN system, with error from standard deviation of N = 3. See Table 1 for symbol designation.

$$K_c = \frac{1.076X_v\left(\frac{t}{l}\right)^{1/2}\left(\frac{E}{H}\right)^{2/3}P_{max}}{c^{3/2}} \quad (5)$$

where X_v is an empirically fit constant, t is the distance from the center to the Berkovich corner, l is the length of the emanating crack, c is the total crack length, and P_{max} is the maximum load.[56] In order to examine how both graft density (σ) and degree of polymerization (N) impact the fracture toughness of these films, Figure 6c plots the measured K_c of the ***MxG*-CNC-*g*-PS** films against N/σ.

Interestingly, all measured samples show higher fracture toughness (K_c) than a 60 kg/mol PS film (60 kg/mol being the highest molecular weight graft used in this study), irrespective of grafting density and degree of polymerization. The mixed nanocomposite sample (**MxG-CNC-COOH** with 90 wt % **PS-NH$_2$-12**) shows a lower fracture toughness (1.3 ± 0.3 MPa·m$^{0.5}$) relative to the PGN films, and akin to that of the homopolymer **PS-NH$_2$-60** (1.7 ± 0.7 MPa·m$^{0.5}$). The PGNs

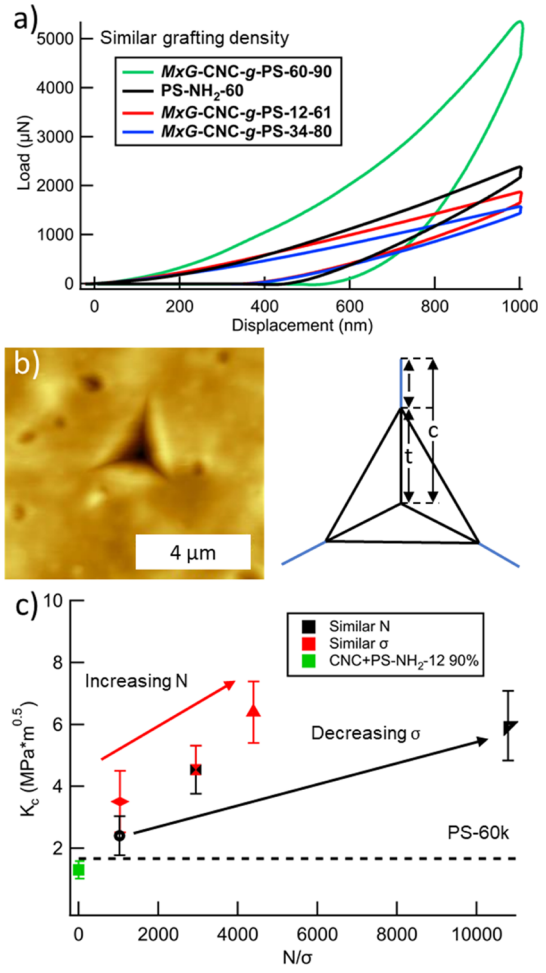

Figure 6. (a) Load−displacement curves obtained by nanoindentation for ***MxG*-CNC-*g*-PS** films with a constant polymer grafting density (σ) but different degrees of polymerization (N) of the graft, (b) AFM of ***MxG*-CNC-*g*-PS-34-80** post-indentation with a schematic of an indentation created using a Berkovich tip where c is the total crack length measured from the center of contact to the end of crack at the sample surface, t is the distance from the center of contact to the corner, and l is the length of the cracks emanating from the corners. (c) Fracture toughness of the ***MxG*-CNC-*g*-PS** film vs divisor of degree of polymerization and grafting density with a measured toughness of 60 k reference PS sample and **MxG-CNC-COOH** with 90 wt % **PS-NH$_2$-12** from N = 10.

with similar grafting density (0.11 chains/nm^2), ***MxG*-CNC-*g*-PS-12-61**, ***MxG*-CNC-*g*-PS-34-80**, and ***MxG*-CNC-*g*-PS-60-90** all show increasing fracture toughness (from 3.5 ± 1.0 MPa·m$^{0.5}$ to 6.4 ± 1.0 MPa·m$^{0.5}$) with the increase in the degree of polymerization. The PGNs with similar molecular weight (ca. 30 kg/mol) and thus degree of polymerization, ***MxG*-CNC-*g*-PS-27-88**, ***MxG*-CNC-*g*-PS-34-80**, and ***MxG*-CNC-*g*-PS-34-55**, all show increasing fracture toughness with the decrease in the grafting density, from 2.4 ± 0.6 MPa·m$^{0.5}$ to 6.0 ± 1.1 MPa·m$^{0.5}$. These data broadly support the predictions of Keten and co-workers,[42] confirming that increasing fracture toughness is obtained with a relatively lower grafting density of higher degree of polymerization polymers.

In seeking to demonstrate the overall mechanical effects of the ***MxG*-CNC-*g*-PS** PGN films, along with homopolymer and a two-component composite, the rubbery modulus was plotted

https://doi.org/10.1021/acs.macromol.1c01886
Macromolecules 2021, 54, 10594−10604

against the fracture toughness (Figure 7) and color being used to highlight the polymer conformation of the PGNs. While

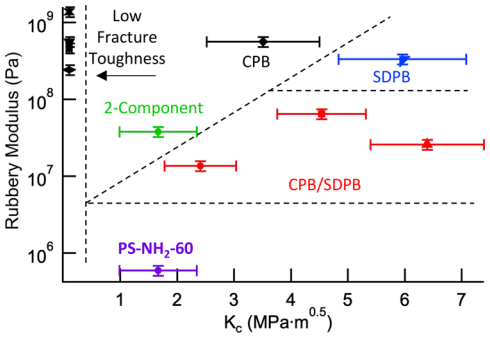

Figure 7. Rubbery modulus as determined by tensile DMA plotted against the fracture toughness as determined by nanoindentation for a variety of PGN, two-component nanocomposite, and homopolymer samples. PGN samples are labeled according to their grafted polymer brush regime. Samples whose fracture toughness could not be calculated are to the far left.

PGNs in the CPB regime form films of high modulus on account of their large nanofiller loading, as high as 55 wt % CNC, their fracture toughness is low. PGNs in the CPB/SDPB regime generally show an enhancement in fracture toughness, the significant quantity of polymer needed to access that regime limits the nanofiller loading and thus the modulus. By accessing a material with both high polymer degree of polymerization and relatively low grafting density, which permits both SDPB conformation and entanglement alongside a high nanofiller loading, it is possible to optimize both the modulus and fracture toughness.

CONCLUSIONS

***MxG*-CNC-*g*-PS** samples were synthesized with a controlled grafted polymer degree of polymerization and density. AFM studies were used to determine the grafted polymer conformation as a function of both degree of polymerization and grafting density, and it was shown that the mechanical properties of these OCNs strongly depend upon the grafted polymer conformation and the total amount of polymer. Specifically, modulus measured by tensile DMA showed that trends of the materials below T_g (glassy) was relatively invariant with composition, while above T_g (rubbery), there is a dramatic improvement in the modulus with the decrease in molecular weight and decreasing grafting density ranging from 13 MPa to 1.37 GPa, which is related to the amount of the CNC in the PGN. The PGN architecture allows access to homogeneous films with as much as 55 wt % CNC, resulting in films with a GPa modulus above T_g. In measuring the T_g, PGNs in the CPB regime displayed T_g values 20 °C higher than comparable ungrafted homopolymer, with the difference in T_g decreasing with the increase in molecular weight. Fracture toughness measured by the nanoindentation of the PGN films showed a significant improvement in their fracture toughness relative to the PS homopolymer of similar degree of polymerization (1.7 ± 0.7 MPa·m$^{0.5}$), with the greatest improvement in fracture toughness with the increase in degree of polymerization and decreasing grafting density (up to 6.4 ± 1.0 MPa·m$^{0.5}$). Ultimately, the PGN films enabled large loadings of nanorod filler (up to 55 wt %) with excellent mechanical properties and provide stronger understanding of the structure property relations of this new class of materials.

ASSOCIATED CONTENT

Supporting Information

The Supporting Information is available free of charge at https://pubs.acs.org/doi/10.1021/acs.macromol.1c01886.

^{1}H NMR, GPC−MALS, and UV−Vis images of **PS-8**; TGA of **PS-5**; ^{1}H NMR and GPC−MALS images of **PS-NH$_2$** samples; homopolymer synthesis summary; TGA, WAXS, AFM, and SEM images of ***MxG*-CNC**; scheme, ^{1}H NMR, and ^{13}C NMR spectra of **DMTMMBF$_4$**; scheme and TGA testing coupling reaction agents; ATR−FTIR and AFM images of ***MxG*-CNC-*g*-PS** samples, linear regression of the CPB data from Figure 2b; rubbery modulus versus polymer weight fraction; DSC of **PS-NH$_2$** samples; comparison tensile DMA and shear rheology of **PS-NH$_2$** and ***MxG*-CNC-*g*-PS**; hardness and modulus data from nanoindentation; and AFM of nanoindentation (PDF)

AUTHOR INFORMATION

Corresponding Authors

Paul F. Nealey − *Pritzker School of Molecular Engineering, University of Chicago, Chicago, Illinois 60637, United States;* orcid.org/0000-0003-3889-142X; Email: nealey@uchicago.edu

Stuart J. Rowan − *Pritzker School of Molecular Engineering, University of Chicago, Chicago, Illinois 60637, United States; Department of Chemistry, University of Chicago, Chicago, Illinois 60637, United States; Chemical and Engineering Sciences Division, Argonne National Laboratory, Lemont, Illinois 60439, United States;* orcid.org/0000-0001-8176-0594; Email: stuartrowan@uchicago.edu

Authors

James H. Lettow − *Pritzker School of Molecular Engineering, University of Chicago, Chicago, Illinois 60637, United States*

Han Yang − *Pritzker School of Molecular Engineering, University of Chicago, Chicago, Illinois 60637, United States;* orcid.org/0000-0003-3971-1734

Complete contact information is available at: https://pubs.acs.org/10.1021/acs.macromol.1c01886

Notes

The authors declare no competing financial interest.

ACKNOWLEDGMENTS

This work was supported by the U.S. Army Research Office (ARO) under grant numbers W911NF-15-1-0190 and W911NF-18-1-0287 and by WAXS experiments, performed at the DuPont-Northwestern-Dow Collaborative Access Team (DND-CAT) located at Sector 5 of the Advanced Photon Source (APS). DND-CAT is supported by Northwestern University, The Dow Chemical Company, and DuPont de Nemours, Inc. This research used resources of the Advanced Photon Source; a U.S. Department of Energy (DOE) Office of Science User Facility operated for the DOE Office of Science by Argonne National Laboratory under contract no. DE-AC02-06CH11357. WAXS data were collected using an instrument funded by the National Science Foundation under award number 0960140. Part of this work made use of the shared

facilities at the University of Chicago Materials Research Science and Engineering Center, supported by National Science Foundation under award number DMR-2011854, and the Soft Matter Characterization Facility of the University of Chicago. Parts of this work made use of the SPID facility of Northwestern University's NUANCE Center, which has received support from the SHyNE Resource (NSF ECCS-2025633), the IIN, and Northwestern's MRSEC program (NSF DMR-1720139). The authors thank Aloterra Energy LLC for the donation of MxG stalks.

■ ABBREVIATIONS

PS, polystyrene; *MxG*, *Miscanthus x. Giganteus*; CNC, cellulose nanocrystal; PNGs, polymer-grafted nanoparticles; OCN, one-component nanocomposite; IL, ionic liquid; ESI−MS, electrospray mass spectroscopy; LC/MS, liquid chromatography/mass spectroscopy; GPC−MALS, gel permeation chromatography−multiangle light scattering; DI, deionized; RAFT, reversible addition fragmentation chain transfer; CTA, chain transfer agent; NMR, nuclear magnetic resonance; AIBN, azobisisobutyronitrile; THF, tetrahydrofuran; WAXS, wide angle X-ray scattering; AFM, atomic force microscopy; SEM, scanning electron microscopy; FTIR, Fourier transform infrared spectroscopy; TGA, thermal gravimetric analysis; RH, relative humidity; CPB, concentrated polymer brush; SDPB, semidilute polymer brush; EISA, evaporation-induced self-assembly; wt %, weight percent

■ REFERENCES

(1) Kumar, S. K.; Benicewicz, B. C.; Vaia, R. A.; Winey, K. I. 50th Anniversary Perspective: Are Polymer Nanocomposites Practical for Applications? *Macromolecules* **2017**, *50*, 714−731.
(2) Bet-Moushoul, E.; Mansourpanah, Y.; Farhadi, K.; Tabatabaei, M. TiO2 Nanocomposite Based Polymeric Membranes: A Review on Performance Improvement for Various Applications in Chemical Engineering Processes. *Chem. Eng. J.* **2016**, *283*, 29−46.
(3) Crosby, A. J.; Lee, J. Y. Polymer Nanocomposites: The "Nano" Effect on Mechanical Properties. *Polym. Rev.* **2007**, *47*, 217−229.
(4) Cammarata, R. C. Mechanical Properties of Nanocomposite Thin Films. *Thin Solid Films* **1994**, *240*, 82−87.
(5) Kumar, A.; Sharma, K.; Dixit, A. R. A Review of the Mechanical and Thermal Properties of Graphene and Its Hybrid Polymer Nanocomposites for Structural Applications. *J. Mater. Sci.* **2019**, *54*, 5992−6026.
(6) Kim, D. J.; Jo, M. J.; Nam, S. Y. A Review of Polymer-Nanocomposite Electrolyte Membranes for Fuel Cell Application. *J. Ind. Eng. Chem.* **2015**, *21*, 36−52.
(7) Gadim, T. D. O.; Vilela, C.; Loureiro, F. J. A.; Silvestre, A. J. D.; Freire, C. S. R.; Figueiredo, F. M. L. Nafion® and Nanocellulose: A Partnership for Greener Polymer Electrolyte Membranes. *Ind. Crops Prod.* **2016**, *93*, 212−218.
(8) Demirocak, D.; Srinivasan, S.; Stefanakos, E. A Review on Nanocomposite Materials for Rechargeable Li-Ion Batteries. *Appl. Sci.* **2017**, *7*, 731−26.
(9) Ashraf, S.; Siddiqa, A.; Shahida, S.; Qaisar, S. Titanium-Based Nanocomposite Materials for Arsenic Removal from Water: A Review. *Heliyon* **2019**, *5*, No. e01577.
(10) Bassyouni, M.; Abdel-Aziz, M. H.; Zoromba, M. S.; Abdel-Hamid, S. M. S.; Drioli, E. A Review of Polymeric Nanocomposite Membranes for Water Purification. *J. Ind. Eng. Chem.* **2019**, *73*, 19−46.
(11) Hore, M. J. A.; Korley, L. T. J.; Kumar, S. K. Polymer-Grafted Nanoparticles. *J. Appl. Phys.* **2020**, *128* (). https://doi.org/DOI: 10.1063/5.0019326.
(12) Fernandes, N. J.; Koerner, H.; Giannelis, E. P.; Vaia, R. A. Hairy Nanoparticle Assemblies as One-Component Functional Polymer Nanocomposites: Opportunities and Challenges. *MRS Commun.* **2013**, *3*, 13−29.
(13) Choi, J.; Hui, C. M.; Pietrasik, J.; Dong, H.; Matyjaszewski, K.; Bockstaller, M. R. Toughening Fragile Matter: Mechanical Properties of Particle Solids Assembled from Polymer-Grafted Hybrid Particles Synthesized by ATRP. *Soft Matter* **2012**, *8*, 4072.
(14) Schmitt, M.; Choi, J.; Hui, C. M.; Chen, B.; Korkmaz, E.; Yan, J.; Margel, S.; Ozdoganlar, O. B.; Matyjaszewski, K.; Bockstaller, M. R. Processing Fragile Matter: Effect of Polymer Graft Modification on the Mechanical Properties and Processibility of (Nano-) Particulate Solids. *Soft Matter* **2016**, *12*, 3527−3537.
(15) Jiao, Y.; Tibbits, A.; Gillman, A.; Hsiao, M.-S.; Buskohl, P.; Drummy, L. F.; Vaia, R. A. Deformation Behavior of Polystyrene-Grafted Nanoparticle Assemblies with Low Grafting Density. *Macromolecules* **2018**, *51*, 7257−7265.
(16) Midya, J.; Cang, Y.; Egorov, S. A.; Matyjaszewski, K.; Bockstaller, M. R.; Nikoubashman, A.; Fytas, G. Disentangling the Role of Chain Conformation on the Mechanics of Polymer Tethered Particle Materials. *Nano Lett.* **2019**, *19*, 2715−2722.
(17) Dan, N.; Tirrell, M. Polymers Tethered to Curved Interfaces. A Self-Consistent-Field Analysis. *Macromolecules* **1992**, *25*, 2890−2895.
(18) Halperin, A.; Tirrell, M.; Lodge, T. P. Tethered Chains in Polymer Microstructures. *Adv. Polym. Sci.* **1991**, *100*, 31−71.
(19) Ohno, K.; Morinaga, T.; Koh, K.; Tsujii, Y.; Fukuda, T. Synthesis of Monodisperse Silica Particles Coated with Well-Defined, High-Density Polymer Brushes by Surface-Initiated Atom Transfer Radical Polymerization. *Macromolecules* **2005**, *38*, 2137−2142.
(20) Tai, Y.; Morinaga, T.; Ohno, K.; Tsujii, Y.; Fukuda, T. Fixation of Colloidal Crystals Formed by Monodisperse Silica Particles Grafted with Concentrated Polymer Brush. *Polym. Preprint.* **2006**, *55*, 3420.
(21) Ohno, K.; Morinaga, T.; Takeno, S.; Tsujii, Y.; Fukuda, T. Suspensions of Silica Particles Grafted with Concentrated Polymer Brush: Effects of Graft Chain Length on Brush Layer Thickness and Colloidal Crystallization. *Macromolecules* **2007**, *40*, 9143−9150.
(22) Julkapli, N. M.; Bagheri, S. Nanocellulose as a Green and Sustainable Emerging Material in Energy Applications: A Review. *Polym. Adv. Technol.* **2017**, *28*, 1583−1594.
(23) Eichhorn, S. J.; Dufresne, A.; Aranguren, M.; Marcovich, N. E.; Capadona, J. R.; Rowan, S. J.; Weder, C.; Thielemans, W.; Roman, M.; Renneckar, S.; Gindl, W.; Veigel, S.; Keckes, J.; Yano, H.; Abe, K.; Nogi, M.; Nakagaito, A. N.; Mangalam, A.; Simonsen, J.; Benight, A. S.; Bismarck, A.; Berglund, L. A.; Peijs, T. Review: Current International Research into Cellulose Nanofibres and Nanocomposites. *J. Mater. Sci.* **2010**, *45*, 1−33.
(24) Mariano, M.; El Kissi, N.; Dufresne, A. Cellulose Nanocrystals and Related Nanocomposites: Review of Some Properties and Challenges. *J. Polym. Sci., Part B: Polym. Phys.* **2014**, *52*, 791−806.
(25) Shojaeiarani, J.; Bajwa, D. S.; Chanda, S. Cellulose Nanocrystal Based Composites: A Review. *Compos. Part C Open Access* **2021**, *5*, 100164.
(26) Calvino, C.; Macke, N.; Kato, R.; Rowan, S. J. Development, Processing and Applications of Bio-Sourced Cellulose Nanocrystal Composites. *Prog. Polym. Sci.* **2020**, *103*, 101221.
(27) Habibi, Y.; Lucia, L. A.; Rojas, O. J. Cellulose Nanocrystals: Chemistry, Self-Assembly, and Applications. *Chem. Rev.* **2010**, *110*, 3479−3500.
(28) Dong, X. M.; Revol, J.-F.; Gray, D. G. Effect of Microcrystallite Preparation Conditions on the Formation of Colloid Crystals of Cellulose. *Cellulose* **1998**, *5*, 19−32.
(29) Zhang, Y.; Edelbrock, A. N.; Rowan, S. J. Effect of Processing Conditions on the Mechanical Properties of Bio-Inspired Mechanical Gradient Nanocomposites. *Eur. Polym. J.* **2019**, *115*, 107−114.
(30) Cudjoe, E.; Hunsen, M.; Xue, Z.; Way, A. E.; Barrios, E.; Olson, R. A.; Hore, M. J. A.; Rowan, S. J. Miscanthus Giganteus: A Commercially Viable Sustainable Source of Cellulose Nanocrystals. *Carbohydr. Polym.* **2017**, *155*, 230−241.
(31) Weiss, A. M.; MacKe, N.; Zhang, Y.; Calvino, C.; Esser-Kahn, A. P.; Rowan, S. J. In Vitro and in Vivo Analyses of the Effects of Source, Length, and Charge on the Cytotoxicity and Immunocompat-

ibility of Cellulose Nanocrystals. *ACS Biomater. Sci. Eng.* **2021**, *7*, 1450−1461.
(32) Cao, X.; Habibi, Y.; Lucia, L. A. One-Pot Polymerization, Surface Grafting, and Processing of Waterborne Polyurethane-Cellulose Nanocrystal Nanocomposites. *J. Mater. Chem.* **2009**, *19*, 7137.
(33) Lin, N.; Dufresne, A. Physical and/or Chemical Compatibilization of Extruded Cellulose Nanocrystal Reinforced Polystyrene Nanocomposites. *Macromolecules* **2013**, *46*, 5570−5583.
(34) Habibi, Y.; Goffin, A.-L.; Schiltz, N.; Duquesne, E.; Dubois, P.; Dufresne, A. Bionanocomposites Based on Poly(ε-Caprolactone)-Grafted Cellulose Nanocrystals by Ring-Opening Polymerization. *J. Mater. Chem.* **2008**, *18*, 5002.
(35) Wohlhauser, S.; Delepierre, G.; Labet, M.; Morandi, G.; Thielemans, W.; Weder, C.; Zoppe, J. O. Grafting Polymers from Cellulose Nanocrystals: Synthesis, Properties, and Applications. *Macromolecules* **2018**, *51*, 6157−6189.
(36) Morandi, G.; Heath, L.; Thielemans, W. Cellulose Nanocrystals Grafted with Polystyrene Chains through Surface-Initiated Atom Transfer Radical Polymerization (SI-ATRP). *Langmuir* **2009**, *25*, 8280−8286.
(37) Roy, D.; Semsarilar, M.; Guthrie, J. T.; Perrier, S. Cellulose Modification by Polymer Grafting: A Review. *Chem. Soc. Rev.* **2009**, *38*, 2046−2064.
(38) Zoppe, J. O.; Xu, X.; Känel, C.; Orsolini, P.; Siqueira, G.; Tingaut, P.; Zimmermann, T.; Klok, H.-A. Effect of Surface Charge on Surface-Initiated Atom Transfer Radical Polymerization from Cellulose Nanocrystals in Aqueous Media. *Biomacromolecules* **2016**, *17*, 1404−1413.
(39) Wohlhauser, S.; Kuhnt, T.; Meesorn, W.; Montero De Espinosa, L.; Zoppe, J. O.; Weder, C. One-Component Nanocomposites Based on Polymer-Grafted Cellulose Nanocrystals. *Macromolecules* **2020**, *53*, 821−834.
(40) Kato, R.; Lettow, J. H.; Patel, S. N.; Rowan, S. J. Ion-Conducting Thermoresponsive Films Based on Polymer-Grafted Cellulose Nanocrystals. *ACS Appl. Mater. Interfaces* **2020**, *12*, 54083−54093.
(41) Lettow, J. H.; Kaplan, R. Y.; Nealey, P. F.; Rowan, S. J. Enhanced Ion Conductivity through Hydrated, Polyelectrolyte-Grafted Cellulose Nanocrystal Films. *Macromolecules* **2021**, *54*, 6925−6936.
(42) Hansoge, N. K.; Huang, T.; Sinko, R.; Xia, W.; Chen, W.; Keten, S. Materials by Design for Stiff and Tough Hairy Nanoparticle Assemblies. *ACS Nano* **2018**, *12*, 7946−7958.
(43) Hansoge, N. K.; Keten, S. Effect of Polymer Chemistry on Chain Conformations in Hairy Nanoparticle Assemblies. *ACS Macro Lett.* **2019**, *8*, 1209−1215.
(44) Postma, A.; Davis, T. P.; Evans, R. A.; Li, G.; Moad, G.; O'Shea, M. S. Synthesis of Well-Defined Polystyrene with Primary Amine End Groups through the Use of Phthalimido-Functional RAFT Agents. *Macromolecules* **2006**, *39*, 5293−5306.
(45) Raw, S. A. An Improved Process for the Synthesis of DMTMM-Based Coupling Reagents. *Tetrahedron Lett.* **2009**, *50*, 946−948.
(46) Pyun, J.; Kowalewski, T.; Matyjaszewski, K. Synthesis of Polymer Brushes Using Atom Transfer Radical Polymerization. *Macromol. Rapid Commun.* **2003**, *24*, 1043−1059.
(47) Fujisawa, S.; Ikeuchi, T.; Takeuchi, M.; Saito, T.; Isogai, A. Superior Reinforcement Effect of TEMPO-Oxidized Cellulose Nanofibrils in Polystyrene Matrix: Optical, Thermal, and Mechanical Studies. *Biomacromolecules* **2012**, *13*, 2188−2194.
(48) Capadona, J. R.; Shanmuganathan, K.; Tyler, D. J.; Rowan, S. J.; Weder, C. Stimuli-Responsive Polymer Nanocomposites Inspired by the Sea Cucumber Dermis. *Science* **2008**, *319*, 1370−1374.
(49) Mendez, J.; Annamalai, P. K.; Eichhorn, S. J.; Rusli, R.; Rowan, S. J.; Foster, E. J.; Weder, C. Bioinspired Mechanically Adaptive Polymer Nanocomposites with Water-Activated Shape-Memory Effect. *Macromolecules* **2011**, *44*, 6827−6835.
(50) Askar, S.; Li, L.; Torkelson, J. M. Polystyrene-Grafted Silica Nanoparticles: Investigating the Molecular Weight Dependence of Glass Transition and Fragility Behavior. *Macromolecules* **2017**, *50*, 1589−1598.
(51) Rittigstein, P.; Priestley, R. D.; Broadbelt, L. J.; Torkelson, J. M. Model Polymer Nanocomposites Provide an Understanding of Confinement Effects in Real Nanocomposites. *Nat. Mater.* **2007**, *6*, 278−282.
(52) Koerner, H.; Opsitnick, E.; Grabowski, C. A.; Drummy, L. F.; Hsiao, M.-S.; Che, J.; Pike, M.; Person, V.; Bockstaller, M. R.; Meth, J. S.; Vaia, R. A. Physical Aging and Glass Transition of Hairy Nanoparticle Assemblies. *J. Polym. Sci., Part B: Polym. Phys.* **2016**, *54*, 319−330.
(53) Dang, A.; Hui, C. M.; Ferebee, R.; Kubiak, J.; Li, T.; Matyjaszewski, K.; Bockstaller, M. R. Thermal Properties of Particle Brush Materials: Effect of Polymer Graft Architecture on the Glass Transition Temperature in Polymer-Grafted Colloidal Systems. *Macromol. Symp.* **2013**, *331*−*332*, 9−16.
(54) Sunday, D. F.; Green, D. L. Thermal and Rheological Behavior of Polymer Grafted Nanoparticles. *Macromolecules* **2015**, *48*, 8651−8659.
(55) Sakib, N.; Koh, Y. P.; Huang, Y.; Mongcopa, K. I. S.; Le, A. N.; Benicewicz, B. C.; Krishnamoorti, R.; Simon, S. L. Thermal and Rheological Analysis of Polystyrene-Grafted Silica Nanocomposites. *Macromolecules* **2020**, *53*, 2123−2135.
(56) Fischer-Cripps, A. C. *Nanoindentation*, 3rd ed.; Springer, 2011.

https://doi.org/10.1021/acs.macromol.1c01886
Macromolecules 2021, 54, 10594−10604